Combination of glucose and oxygen gradients dictates metabolic regime and antibiotic tolerance of biofilms

Shouxian Hu[a], Yulin Zhao[a], Jintao Liu[a,b]*

[a] Center for Infection Biology, School of Basic Medical Sciences, Tsinghua University, Beijing 100084, China

[b] SXMU-Tsinghua Collaborative Innovation Center for Frontier Medicine, Shanxi Medical University, Taiyuan, Shanxi Province 030001, China

* Address correspondence to: JintaoLiu@tsinghua.edu.cn

Abstract

Biofilms are structured bacterial communities that underlie many persistent infections, exhibiting strong survival under antibiotics that cannot be explained by genetic resistance alone. Here we uncover a biofilm-specific mechanism of antibiotic tolerance driven by spatial gradients. Using an agarose-based *Escherichia coli* biofilm system, we found a non-monotonic relationship between glucose availability and biofilm growth: high glucose paradoxically reduced final biomass. This arose from the overlap of the glucose penetration zone and the anaerobic core of the biofilm at high glucose, triggering mixed-acid fermentation. We identified acetate, a fermentation by-product secreted by the biofilm, as a potent inducer of tolerance to gentamicin and ciprofloxacin. This effect was biofilm-specific: acetate enhanced antibiotic killing instead of tolerance in planktonic cultures. In biofilms, acetate entered the TCA cycle via the glyoxylate shunt, driving respiration that depleted oxygen and maintained a persistent anaerobic core, thereby blocking antibiotic efficacy. Supplementing the alternative electron acceptor fumarate fully reversed biofilm tolerance. Our work demonstrates that community-level metabolic organization can invert the relationship between metabolic activity and antibiotic susceptibility, and reveals that interventions effective against planktonic bacteria may be counterproductive in biofilms. These findings underscore the necessity of considering spatial physiology in the development of anti-biofilm therapies.

Introduction

Antibiotics are the main drugs for treating bacterial infections. However, failures of antibiotic therapies have increasingly become a problem. A common cause of failure is antibiotic resistance, in which the bacteria acquire mutations or resistance genes that make existing antibiotics ineffective[1]. Therefore, many efforts have been devoted to developing new antibiotics[2-5]. While those efforts are important, a major limitation is that they cannot solve another important cause of failure – bacteria that are sensitive to antibiotics are not always fully eradicated by the drugs, resulting in relapse of infections[6]. This tolerance to antibiotics usually leads to prolonged treatments. Given that bacteria can evolve rapidly, the prolonged treatments often promote the evolution of resistance[7,8]. This problem cannot be solved by the development of new antibiotics, as they eventually also fall into the same cycle. To break this dilemma, it is important to avoid antibiotic tolerance in the first place, so that prolonged treatments can be minimized.

A common cause of antibiotic tolerance is biofilms, which are structured bacterial communities[9]. Biofilms are notoriously resilient to antibiotics, often surviving concentrations hundreds of times higher than their planktonic counterparts[10,11]. Studies suggest that biofilm tolerance is multifactorial: poor antibiotic penetration due to extracellular matrix[12-14], slow growth due to nutrient limitation[15,16], hypoxia due to oxygen consumption[17,18], and stress response activation[11,19,20]. These explanations reduce biofilm properties to that of the cellular-level. However, biofilms can also give rise to community-level properties that do not exist at the cellular-level[21-24]. Therefore, it is an open question whether antibiotic interventions could be improved based on community-level understandings.

Here, we took a community-based approach and perceive each biofilm as an integral unit. This prompted us to study the internal structure of biofilms. Due to the dense packing of the bacteria, spatial gradients emerge in biofilms[25,26]. As a consequence, a biofilm differentiates into physiologically distinct subpopulations, exhibiting spatial heterogeneity that is absent in planktonic bacteria[27,28]. We found that different combinations of gradients lead to different types of biofilms, which shaped the environment in different ways. The environment in turn resulted in different outcomes in antibiotic tolerance. Interestingly, the tolerance was biofilm-specific. Interventions that promote killing of

planktonic bacteria in contrast promote tolerance in biofilms, showing that it is essential to develop interventions based on the spatial physiology of biofilms.

Results

E. coli biofilms showed non-monotonic relationship between initial glucose and final biomass

We used an agarose-based system to culture biofilms (Fig. 1a, Methods), which has been used in various studies[29-31]. Specifically, we seeded *Escherichia coli* BW25113 in melted agarose with M9 medium. When the agarose solidified, the bacteria were immobilized and each cell grew into a single biofilm (Fig. 1b). We used low-melting agarose and seeded the bacteria at ~37 °C, so that we could avoid unnecessary heat shock to the bacteria during inoculation. We chose an agarose concentration of 0.4%, so that the biofilms are spherical and have well-defined boundaries (Extended Data Fig. 1a), which avoids complications that could introduce variations that hinder quantitative study. We used low inoculation density (10^3 CFU/mL), so that each biofilm had sufficient amount of nutrient to grow into significant size (Extended Data Fig. 1b). We used 96-well plates and a thin layer (~375 µm) of agarose in each well, so that the biofilm sizes were uniform across the depth of the system (Extended Data Fig. 1c).

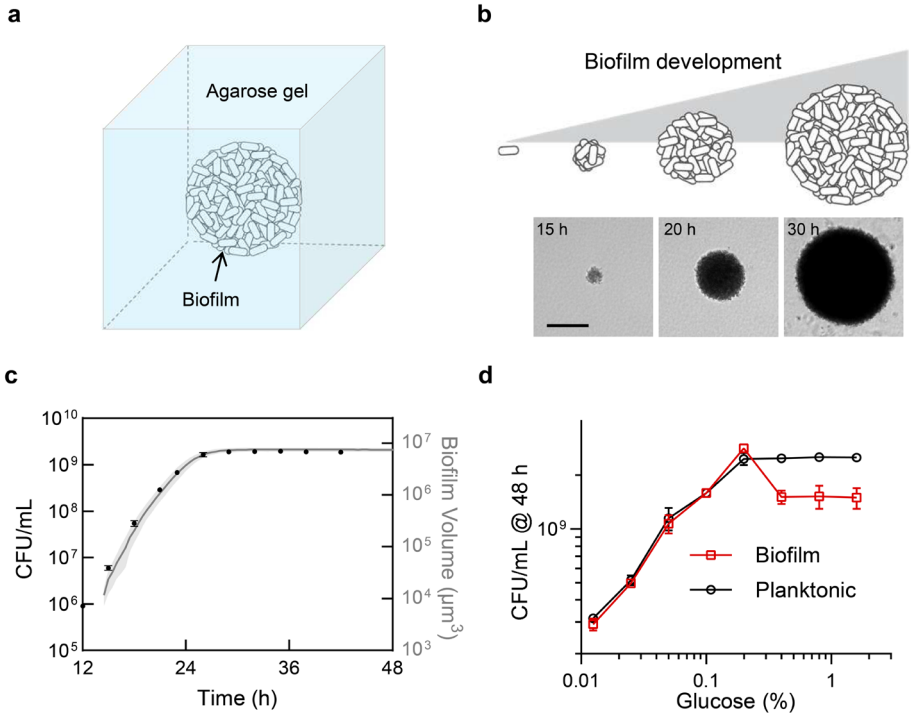

Fig. 1: High glucose availability counterintuitively restricted biofilm growth. a, Schematic of the 3D agarose-based biofilm culturing system. The blue color represents the agarose gel, and the arrow indicates a confined biofilm. **b**, Phase contrast images showing the growth of a biofilm started from a single bacterium. Scale bar,

100 μm. **c**, Growth curve of the biofilm as measure by CFU (left y-axis) and biofilm volume (right y-axis). It shows a typical transition from exponential expansion to stationary phase. Representative of at least three biological replicates. **d**, Stationary-phase CFU of biofilm and planktonic cultures across a broad range of initial glucose concentrations. While planktonic growth saturates at high glucose levels, biofilm growth exhibits a non-monotonic relation with glucose, with high initial glucose (>0.2%, w/v) counterintuitively led to low final CFU. *n* = 3 biological replicates for all the experiments. Error bars indicate mean values +/- SD.

Having established the experimental system, we measured the growth of the biofilms. Similar to in planktonic culture, the biofilms initially grew exponentially and eventually reached stationary phase (Fig. 1c). We quantified biofilm growth using both Colony Forming Unit (CFU) and volume (Methods), and found that CFU is proportional to biofilm volume (Extended Data Fig. 2a), showing that CFU is a good measure of biofilm biomass. Therefore, for the rest of the study we used CFU as our primary metric to quantify biofilms, which has the advantage of being suitable for counting bacterial numbers spanning across orders of magnitudes. We measured the CFUs of stationary phase biofilms started with various initial concentrations of glucose – the only carbon source in the growth medium. Consistent with more nutrient leading to more biomass, the stationary phase CFU was proportional to initial glucose until the latter reached 0.2% (w/v) (Fig. 1d, Extended Data Fig. 2b). However, in contrast to our expectation that the CFU increase with glucose would eventually level off due to saturation, we found higher initial glucose (>0.2%) counterintuitively led to lower final CFU than 0.2% glucose (Fig. 1d). We repeated the experiment with planktonic culture, and found the final CFU leveled off instead of decreased at high glucose (Fig. 1d). Therefore, the non-monotonic relation between initial glucose and final CFU is biofilm-specific.

Combination of glucose and oxygen gradients gave rise to two metabolic regimes in the biofilm

The difference between biofilm and planktonic culture provides an important clue. In planktonic culture, the bacteria are sparsely distributed and all the cells experience the same environment. In contrast, in biofilms, the bacteria are densely packed and there are spatial gradients in the colony[32]. Since glucose is consumed while diffusing into the biofilm, its penetration into the biofilm could be limited, and higher glucose concentration would result in deeper penetration. However, glucose gradient alone is not sufficient to explain the non-monotonic relation shown above, and there must

be other factors involved. We noticed that there are also oxygen gradients in the biofilms, and often the interior regions of biofilms are anaerobic[25,33]. With both glucose and oxygen gradients present in the biofilms, there are two regimes (Fig. 2a): at low glucose concentration, the penetration of glucose into the biofilms is shallow, and there would be no overlap between the glucose zone and the anaerobic zone; at high glucose concentration, the penetration of glucose is deep enough that there would be overlap between the two zones. In the latter case, the bacteria in the overlapping zone would utilize glucose through mix-acid fermentation due to lack of oxygen, and secrete metabolites that reduce the pH of the environment[34]. Therefore, we speculated that the non-monotonic relation was caused by drop of pH under the second regime.

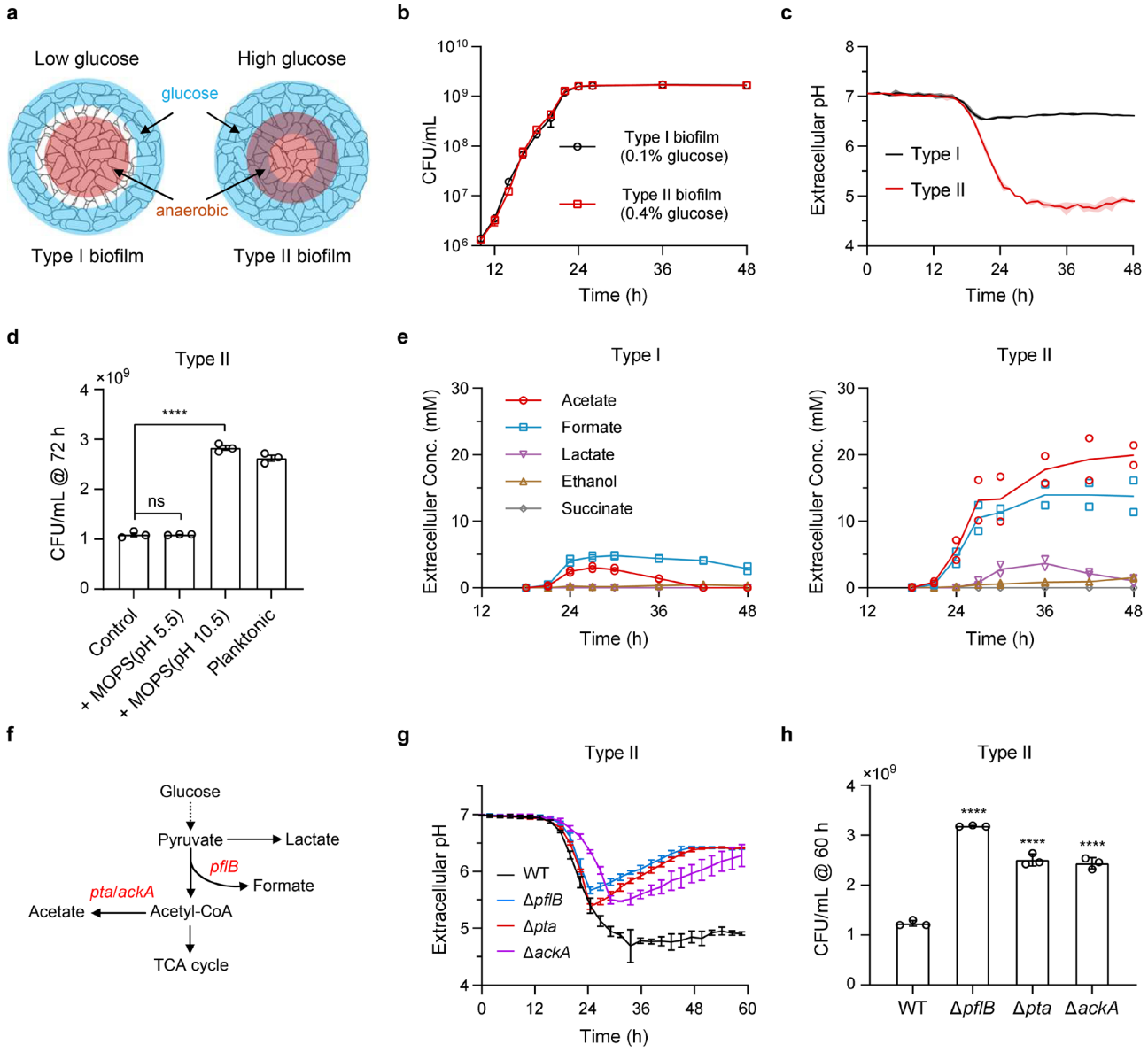

Fig. 2: Combination of glucose and oxygen gradients gave rise to two metabolic regimes in the biofilm. a, Schematic illustrating combination of glucose and oxygen gradients leads to two types of biofilms, as

distinguished by the absence (type I) and presence (type II) of overlap between the glucose zone and the anaerobic zone. Blue indicates the biofilm regions with glucose, and red indicates regions lacking oxygen. **b**, Growth curves of representative type I (0.1% initial glucose) and type II (0.4% initial glucose) biofilms respectively. **c**, Dynamics of extracellular pH during the growth of the biofilms. Type II biofilms caused significant drop of pH in late exponential phase. **d**, Effect of MOPS buffer on the final CFU. The buffer was added at 48 h, the CFU was measured at 72 h. The buffer with pH 10.5 adjusted extracellular pH to 7 (Extended Data Fig. 4b). The planktonic control was performed with the same initial glucose without added buffer. **e**, Concentration of extracellular metabolites during the growth of the biofilms. Type II biofilms showed high accumulation of acetate and formate. n = 2 biological replicates. **f**, Diagram of a simplified pathway for glucose fermentation in *E. coli*. **g**–**h**, Knocking out the key genes for formate or acetate synthesis resulted in transient drop of extracellular pH and increase of final CFU in type II biofilm. n = 3 biological replicates for all the experiments (except for e). Error bars indicate mean values +/- SD. Statistical significance was determined by one-way ANOVA with Dunnett's multiple-comparisons test (**** $p < 0.0001$, ns: no significant).

To test the two-regime hypothesis, we measured the extracellular pH. Specifically, we focused on two representative initial glucose concentrations – 0.1% and 0.4%, which reside on the increasing and decreasing sides of the CFU vs. glucose curve respectively (Fig. 1d). For convenience, we call the corresponding biofilms type I and II respectively. The growth curves of the two types of biofilms are almost identical (Fig. 2b), making it convenient to directly compare them. We measured the extracellular pH during the course of biofilm growth, using the pH-sensitive fluorescent dye BCECF[35] (Extended Data Fig. 3, Methods). Consistent with our speculation, type II biofilm caused a large drop in extracellular pH during late growth phase, which dropped to below 5 (Fig. 2c). In contrast, type I biofilm only caused a <0.5 drop from pH 7 (Fig. 2c). We confirmed that similar pH changes happened with other glucose concentrations in the two regimes respectively (Extended Data Fig. 4a). Using MOPS buffer, we adjusted stationary type II biofilm back to pH 7 (Extended Data Fig. 4b), the biofilm resumed growth and eventually reached CFU values that match that of the corresponding planktonic culture (Fig. 2d). These results show that the non-monotonic relation was due to drop of pH caused by type II biofilm.

We went further to identify the pathway that caused the large drop in pH. According to our hypothesis, the overlapping zone in type II biofilm performs mix-acid fermentation of glucose, which should secrete formate, acetate, lactate, succinate, and ethanol[34]. Therefore, we measured these

metabolites using HPLC (Methods). Consistent with our expectation, type II biofilm started to secrete formate and acetate in late growth phase, and their extracellular concentrations reached ~15 and ~20 mM respectively in stationary phase (Fig. 2e). The accumulation of lactate, succinate, and ethanol was much less and was only transient. In contrast, type I biofilm only secreted <5 mM of acetate and formate, and then consumed them in stationary phase (Fig. 2e).

Under anaerobic condition, *E. coli* generates formate and acetate using the *pflB* and *pta*/*ackA* genes respectively[36,37] (Fig. 2f). Therefore, we cultured type II biofilms using the corresponding knockout strains. We found that they only caused transient drop of pH in late growth phase, and the pH recovered to ~6.5 in stationary phase (Fig. 2g). HPLC experiment suggested that the transient dynamics was due to accumulation and then consumption of lactate by the biofilm (Extended Data Fig. 4c). Consistent with the transient drop of pH, we found the knockout strains could reach 2-3 times higher CFU than the wild type under the type II condition (Fig. 2h).

Acetate secreted under the high-glucose regime promoted biofilm tolerance to antibiotics

The results above show that different combinations of glucose and oxygen gradients give rise to biofilms with different modes of metabolism, and the biofilms shape the environment in different ways by secreting different metabolites. The environment in turn caused different effects on the biofilm. We have seen the effects on biofilm growth. We wonder whether it also causes different effects on the survival of the biofilm, such as under antibiotics.

We treated stationary phase (36 h) biofilms with ampicillin, gentamicin (GEN), and ciprofloxacin respectively (Fig. 3a), which represent three major classes of antibiotics that kill planktonic bacteria with high efficacy[38]. To rule out the effect of pH on antibiotic efficacy, which is relatively trivial, we used MOPS buffer from the start of the experiment (Fig. 3a). We have confirmed that the buffer could avoid significant drop of pH by both type I and II biofilms (Fig. 3b), so that the effect of pH change on antibiotic efficacy is negligible (Extended Data Fig. 5a, b). We counted the percentage of bacteria that survived 24 h of antibiotics (Methods). Ampicillin did not cause much cell death in the biofilm (Fig. 3c, Extended Data Fig. 6a), which is consistent with its dependence on bacterial growth. In contrast, gentamicin and ciprofloxacin showed significant killing efficacy, but only in type I biofilms; type II

biofilms showed high levels of tolerance to these two antibiotics (Fig. 3d-e, Extended Data Fig. 6b-c). These results show that the different environment-shaping effects of the biofilm does in turn lead to different outcomes on the survival of the biofilm.

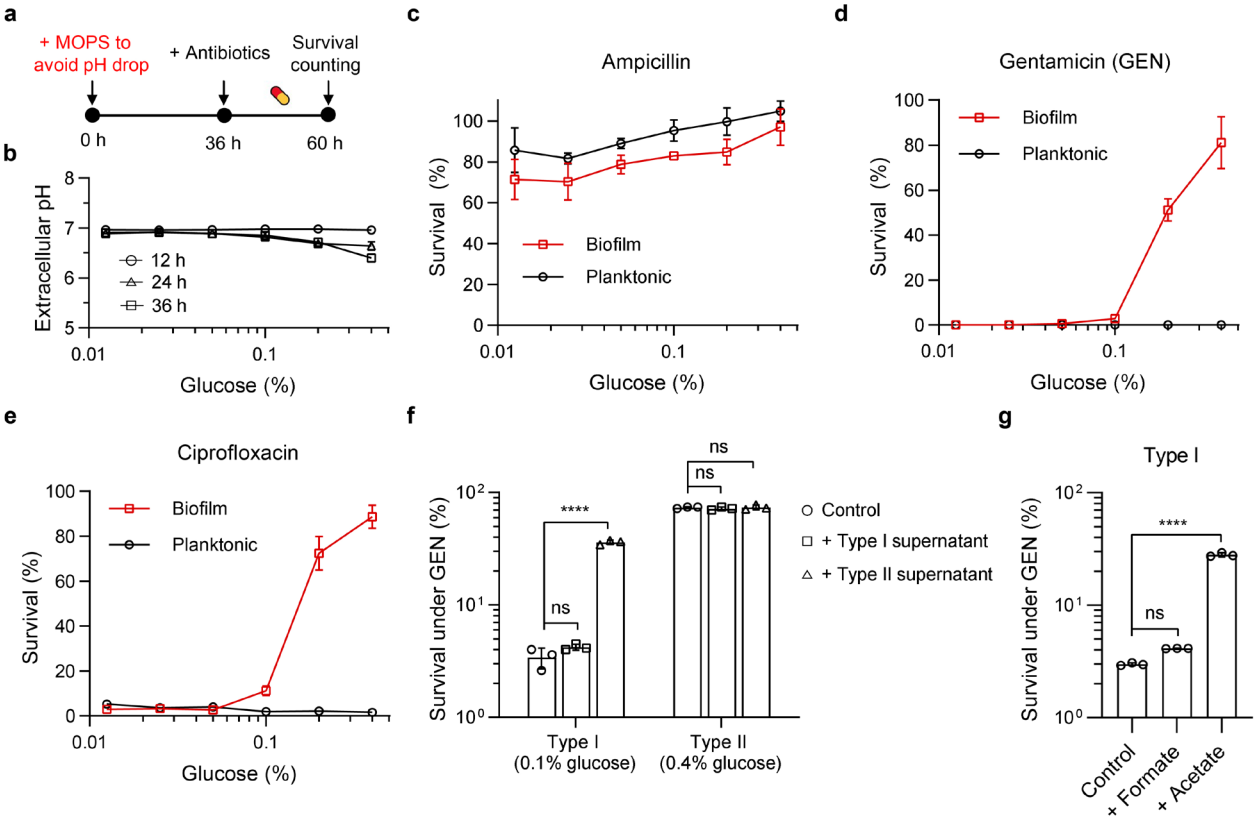

Fig. 3: The two metabolic regimes gave rise to divergent tolerance to antibiotics. a, Schematic of the antibiotic challenge assay. Stationary-phase biofilms (36 h) were treated with antibiotics for 24 h. MOPS buffer was added at the very start of the experiment to rule out the effect of pH. **b**, Profile of extracellular pH under the MOPS buffer. The pH was closely enough to 7 that its influence on antibiotic efficacy is negligible. **c**–**e**, Survival of bacteria after 24 h of antibiotic treatment (ampicillin, 50 μg/mL; gentamicin, 128 μg/mL; ciprofloxacin, 0.5 μg/mL). Type II biofilms showed high tolerance to gentamicin and ciprofloxacin. The planktonic control was performed with the same antibiotic challenge assay. **f**, Effect of supernatants from 36 h biofilm on the survival of the biofilms. Supernatants were added together with the antibiotic (gentamicin, 128 μg/mL). Supernatant from type II biofilm promoted survival of type I biofilm. **g**, Effect of formate or acetate on the survival of type I biofilm. The metabolites (formate, 20 mM; acetate, 20 mM) were added together with the antibiotic (gentamicin, 128 μg/mL). Acetate showed large promotion of biofilm survival. n = 3 biological replicates for all the experiments. Error bars indicate mean values +/- SD. Statistical significance was determined by two-tailed unpaired Student's t-test (**f**) and one-way ANOVA with Dunnett's multiple-comparisons test (**g**) (**** p < 0.0001, ns: no significant).

We hypothesized that certain metabolites secreted by the bacteria promoted the tolerance of type II biofilms. To test this hypothesis, we extracted supernatant from 36 h old type II biofilms (Methods),

and supplemented it to 36 h old type I biofilms and treated the latter with gentamicin. We found the supernatant boosted bacterial survival from ~3% to ~40% (Fig. 3f). We verified that the supernatant from type I biofilm did not boost the survival of itself, nor did it reduce the survival of type II biofilm (Fig. 3f). These results show that certain metabolites secreted by type II biofilm promoted its tolerance. Since type II biofilm accumulated much higher levels of formate and acetate than type I (Fig. 2e), we supplemented 36 h old type I biofilms with formate and acetate (20 mM, matching the concentration detected in type II supernatant) and treated them with gentamicin. We found that acetate increased biofilm survival to a similar level as that by type II supernatant, while formate did not have much effect (Fig. 3g). This suggests that acetate was the main metabolite promoting tolerance in type II biofilm.

Acetate promoted tolerance by maintaining a persistent anaerobic core

Now the question is how does acetate promote biofilm tolerance. *E. coli* uses acetate to synthesize acetyl-CoA, through the *acs* or *ackA*/*pta* pathway[37] (Fig. 4a). We knocked out both pathways, and the effect of acetate was gone (Fig. 4b). Therefore, the synthesis of acetyl-CoA through acetate is essential for the promotion of tolerance. Acetyl-CoA is the entry point for several processes, such as fatty acid synthesis and polyamine acetylation[39,40]. But blocking the corresponding pathways (Δ*fabH* or Δ*speG*) did not abolish the effect of acetate (Extended Data Fig. 7a). Acetyl-CoA is also the entry point for TCA cycle. With acetate but no glucose, *E. coli* activates the glyoxylate shunt[41,42] (Fig. 4a). We found blocking the glyoxylate shunt (Δ*aceA*) abolished the effect of acetate (Fig. 4b), and biofilm tolerance can be recovered by supplementing glyoxylate or succinate – the products of the glyoxylate shunt (Fig. 4c). The glyoxylate shunt further feeds gluconeogenesis (Fig. 4a), which supports the production of biomass[43], but blocking gluconeogenesis (Δ*pck*Δ*pps*) did not abolish the effect of acetate (Fig. 4b). These results show that acetate promotes tolerance by driving the TCA cycle through the glyoxylate shunt.

Normally, activating the TCA cycle promotes the efficacy of antibiotics[44,45]. Indeed, acetate promoted killing of planktonic bacteria by gentamicin (Extended Data Fig. 7b). However, our results above show that it was the opposite in biofilms. We wondered whether this difference was caused by change of

bacterial states in the biofilm. To test this possibility, we dispersed the biofilm during gentamicin treatment (Methods). We found that, acetate switched from promoting tolerance to reducing tolerance once the biofilms were dispersed into individual bacteria (Fig. 4d). This shows that the tolerance promoting effect of acetate was not a property on the single-cell level but emerged in the context of biofilms.

The biofilm-specific effect of acetate prompted us to focus on the spatial properties of biofilms. We have shown that acetate promotes tolerance by driving the TCA cycle through the glyoxylate shunt. The TCA cycle generates NADH and $FADH_2$, which enter the electron transport chain and consumes oxygen[46]. Therefore, we suspected that acetate kept the biofilm interior anaerobic. To track oxygen level in the biofilm, we incorporated an oxygen sensor in the bacteria (Fig. 4e, Methods). The sensor is based-on a Fluorogen-Activating Protein (FAP) system consisting of the DL5 protein and its ligand malachite green[47] (MG). Unlike traditional fluorescent proteins, this system does not require oxygen for maturation. We expressed DL5 under the *fnrF8* promoter, which is activated under anaerobic condition[48] (Extended Data Fig. 7c). Using this sensor, we could see that the interior region of type I biofilm was anaerobic in the growth phase but became aerobic in stationary phase; in contrast, the interior region of type II biofilm stayed anaerobic throughout the entire process (Fig. 4f-g, Methods). This is consistent with the low and high accumulation of acetate in the two types of biofilms respectively (Extended Data Fig. 8a, b). In addition, we saw that supplementing acetate made stationary phase type I biofilm went back to being anaerobic (Fig. 4h). These results show that acetate kept biofilm interior anaerobic.

Lack of oxygen can reduce the efficacy of gentamicin, as its accumulation in the bacteria requires respiration[49]. This may be how acetate promoted tolerance. Then we should be able to reduce the tolerance by providing alternative electron acceptor. Consistent with our expectation, supplementing fumarate completely abolished the promotion of tolerance by acetate in type I biofilm (Fig. 4i), and reduced the tolerance of type II biofilm to the same level as that in type I (Fig. 4j). Knocking out the fumarate reductase (Δ*frdA*) eliminated these effects (Fig. 4k-l), confirming that fumarate exerted its effect as an electron acceptor[50,51] (Extended Data Fig. 9). These results show that acetate promoted

244 tolerance by keeping biofilm interior anaerobic (Fig. 4m). Finally, we confirmed that the biofilm
245 generated tolerance to ciprofloxacin through the same mechanism (Extended Data Fig. 10a-d).

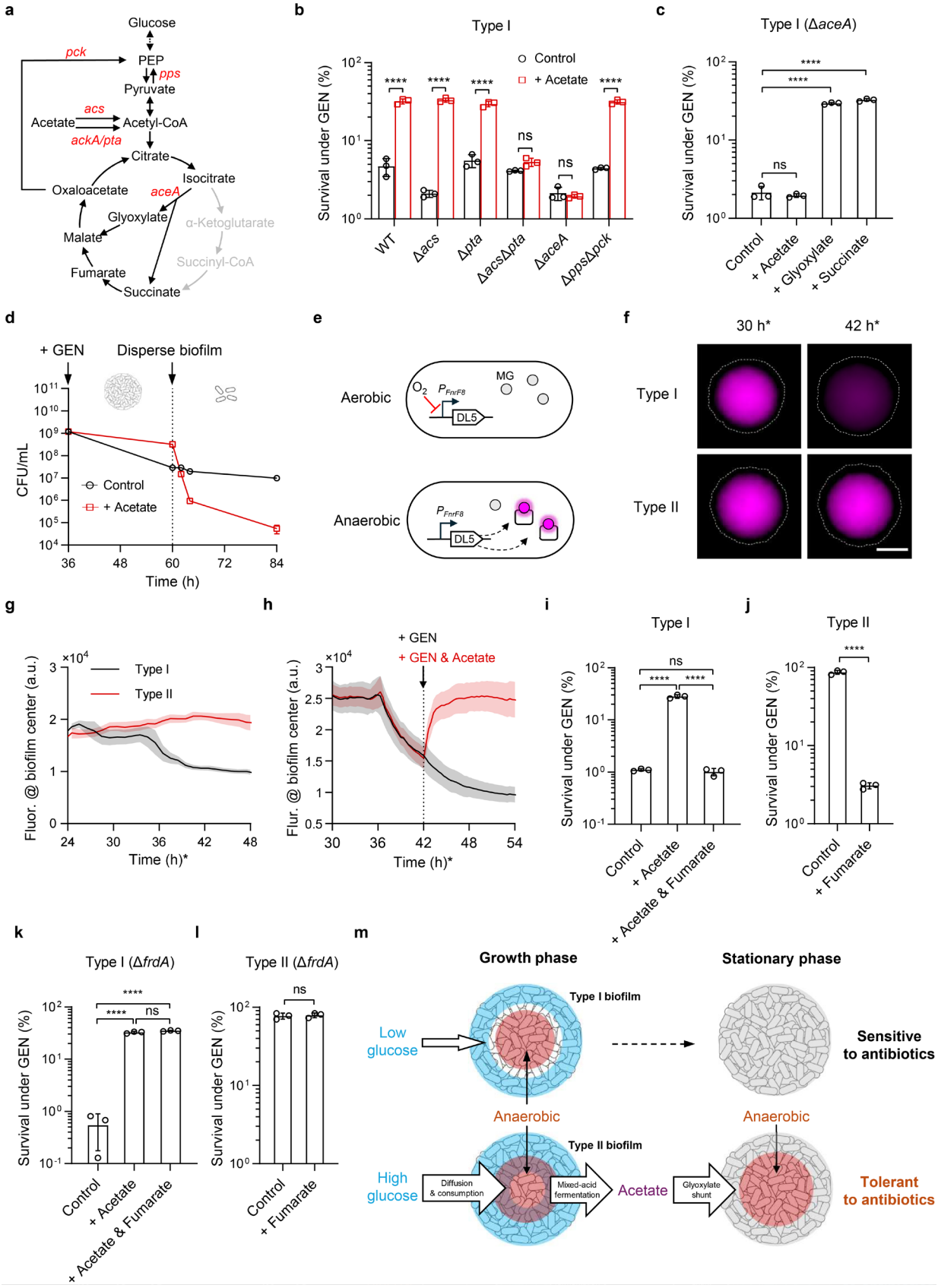

246 **Fig. 4: Acetate secreted under the high-glucose regime promoted biofilm tolerance by maintaining a**

persistent anaerobic core. a, Diagram of a simplified pathway for acetate metabolism in *E. coli*. **b**, Genetic ablation of acetate assimilation (Δ*acs*Δ*pta*) or the glyoxylate shunt (Δ*aceA*) completely abolishes acetate-induced tolerance. **c**, Blocking the glyoxylate shunt abolished the promotion tolerance by acetate, but exogenous addition of the product of the glyoxylate shunt (glyoxylate or succinate) rescued the tolerance. **d**, The protective effect of acetate is biofilm-specific: physically dispersing the biofilm during antibiotic treatment converts acetate from tolerance-promoting to death-promoting. **e**, Schematic of the anaerobic sensor, consisting the fluorogen-activating protein DL5 and its ligand malachite green (MG). DL5 is expressed under anaerobic conditions and MG becomes fluorescent when bound to DL5. **f**–**g**, Fluorescence images (**f**) and fluorescence profiles (**g**) of biofilms formed by the anaerobic sensor strain. Representative of at least three biological replicates. The interior region of type I biofilm became aerobic at stationary phase, while type II biofilm stayed anaerobic. The * sign next to the time indicates that the biofilms entered stationary phase later than the wild type biofilms, as the growth of the sensor strain was slower. Scale bar, 100 μm. **h**, Acetate supplementation reverted the interior of type I biofilms back to anaerobic. **i**, Fumarate supplementation abolished the promotion of tolerance by acetate in type I biofilm. **j**, Fumarate supplementation reduced the tolerance of type II biofilm to the same level as type I. **k**-**l**, Knocking out the fumarate reductase (Δ*frdA*) abolished the tolerance-reduction effect of fumarate. **m**, Model showing how different combinations of glucose and oxygen gradients give rise to different tolerance to antibiotics. Blue indicates the biofilm regions with glucose, and red indicates regions lacking oxygen. For experiments involving antibiotic treatments and metabolite supplementation (**b**-**d**, **h**-**l**), gentamicin was applied at a final concentration of 128 μg/mL, and all exogenous metabolites (acetate, glyoxylate, succinate, and fumarate) were supplemented at 20 mM. $n = 3$ (**b**-**d**; **i**-**l**) or 4 (g, h) biological replicates. Error bars indicate mean values +/- SD. Statistical significance was determined by two-tailed unpaired Student's *t*-test (**** $p < 0.0001$, ns: no significant).

Discussion

We used an agarose-based culturing system, and measured the growth of the biofilm. We found a non-monotonic relation between initial glucose and final CFU – high initial glucose counterintuitively led to low final CFU. We showed that this non-monotonic relationship was biofilm-specific, and was caused by combinations of glucose and oxygen gradients, which led to two metabolic regimes: at low initial glucose, the penetration of glucose into the biofilms is shallow, and there is no overlap between the glucose zone and the anaerobic zone (type I biofilm); at high initial glucose, the penetration of glucose is deep enough that there is overlap between the two zones (type II biofilm). In the latter case, the bacteria in the overlapping zone utilized glucose through mixed-acid fermentation and shaped the environment in different ways from type I biofilm by secreting different metabolites. The environment in turn caused different effects on the biofilm. We further found that type II biofilm

showed much higher tolerance to antibiotics than type I, and identified acetate as the main metabolite promoting tolerance. We showed that acetate promoted tolerance by driving the TCA cycle through the glyoxylate shunt. Interestingly, the tolerance promoting effect of acetate was not a property on the single-cell level but emerged in the context of biofilms. Acetate promoted tolerance by keeping the biofilm interior anaerobic, and supplementing alternative electron acceptor abolished the tolerance.

Our work shows that different combinations of spatial gradients lead to biofilms with different physiological properties. For simplicity, we took a static view of spatial gradients in our model. We do notice that the penetration depths of glucose and oxygen change during biofilm development. As glucose is consumed by the bacteria, its penetration into the biofilm decreases over time. Therefore, the glucose-anaerobic overlapping zone in type II biofilm shrinks over time, and eventually type II biofilm becomes type I. Our classification of biofilms is based on the overall effect of the biofilm on the environment, namely whether the duration of the overlap is long enough that the biofilm secretes sufficient amount of fermentation by-products. The dynamic evolution of spatial gradients and their combinations warrants further study, ideally with the assistance of quantitative modelling.

A major hurdle in treating biofilm infections is that, while antibiotic susceptibility testing is routine for planktonic bacteria, there is still a lack of standards for biofilms. We found that the two types of biofilms showed contrasting tolerance to antibiotics. While type I biofilm was as sensitive to the antibiotics as planktonic bacteria, type II biofilms showed high tolerance. This suggests that understanding biofilm physiology, especially its spatial structure can help us to reach a consensus in biofilm testing standards.

Our work also demonstrates that interventions based on planktonic thinking are not always effective at the community-level. Normally, promoting metabolic activity can sensitize the bacteria to antibiotics[52-54]. However, in biofilms, acetate counterintuitively made the bacteria more tolerant. We found it was because the promotion of metabolic activity sustained the oxygen limitation at the biofilm interior. This demonstrates that understanding the spatial structure of biofilm physiology is also important for effective treatment of biofilms. Finally, there are gradients of various factors in

biofilms. Here we only considered two of the factors – carbon source and oxygen. A systematic investigation of all the major factors and their combinations would help us to better diagnose and treat biofilm infections.

Methods

Bacterial strains and culture conditions. The bacterial strain used in this study was *Escherichia coli* K-12 BW25113. Single-gene knockout mutants were generated using the λ-Red recombination method[55,56]. The antibiotic resistance markers were subsequently excised using the FLP recombinase plasmid pCP20. All strains used in this study are listed in Supplementary Table 1. Luria-Bertani (LB) broth (10 g L^{-1} tryptone, 5 g L^{-1} yeast extract, 10 g L^{-1} NaCl) was used for molecular cloning and routine cultivation. M9 minimal medium was used for both planktonic and biofilm cultures, prepared according to the Cold Spring Harbor protocol: 47.76 mM Na_2HPO_4, 22 mM KH_2PO_4, 18.7 mM NH_4Cl, 8.51 mM NaCl, 2 mM $MgSO_4$, and 0.1 mM $CaCl_2$. Glucose (22 mM) was used as the carbon source. When necessary, antibiotics were added for plasmid maintenance at the following concentrations: chloramphenicol (15 μg mL^{-1}) and kanamycin (25 μg mL^{-1}).

Plasmid construction. The anaerobic biosensor plasmid P_{FnrF8}-DL5 was constructed by assembling three DNA fragments: a chloramphenicol-resistant backbone harboring a p15A origin of replication (modified from iGEM part #BBa_J23119 by replacing the original ColE1 replicon), an anaerobiosis-responsive promoter sequence (P_{FnrF8}) was synthesized based on Liu et al[48], and a gene sequence encoding the fluorogen-activating protein DL5 was codon-optimized and synthesized based on Jojo et al[47]. These fragments were amplified using Q5 High-Fidelity DNA Polymerase (NEB) with primers designed to introduce 20-25 bp of overlapping homologous sequences. Following agarose gel purification, the fragments were assembled at an equimolar ratio using a TEDA-based Gibson assembly mix (incubated at 30 °C for 40 min). The resulting assembly product was transformed into chemically competent *Escherichia coli* K-12 BW25113 cells via heat shock (42 °C for 90 s). Transformants were then recovered and selected on Luria-Bertani (LB) agar plates supplemented with chloramphenicol, and the successful construction of the P_{FnrF8}-DL5 plasmid was verified by whole-plasmid sequencing.

Planktonic culture. A single colony was picked from a fresh agar plate, inoculated into 2 mL of M9 medium, and cultured overnight at 37 °C with shaking. The overnight culture was diluted 1:100 into fresh M9 medium and grown to the exponential phase. A 1 mL aliquot was centrifuged at 5,000 x *g* for 2 min, and the supernatant was discarded. The pellet was resuspended in 1 mL of phosphate-buffered saline (PBS) and adjusted to an OD_{600} of ~0.5. This suspension was serially diluted (1:10,000) in PBS, then inoculated at a 1:100 ratio into fresh M9 medium in the 96-well plate. Growth was monitored by measuring OD_{600} every 15 min using the Spark multimode microplate reader (Tecan).

Agarose block biofilm assay. For biofilm culture, M9 medium was solidified using agarose. A 2% (w/v) stock solution of low-melting-point agarose (Solarbio) was autoclaved and stored at room temperature. Prior to use, the agarose was liquefied at 85 °C for 30 min and cooled down to 37 °C in an incubator. In the meantime, 2× M9 medium (without glucose) was pre-warmed at 37 °C for 10 min. Then the agarose solution, 2× M9 medium, and glucose were mixed to achieve the desired final agarose and glucose concentrations, and kept at 37 °C to prevent premature solidification. Bacterial cells, grown to the mid-exponential phase (OD_{600} ~ 0.5) in M9 medium, were washed with PBS and serially diluted to the desired seeding density. These standardized bacterial suspensions were then uniformly dispersed into the 37 °C liquid M9-agarose mixture. The inoculated matrix was immediately dispensed into 96-well plates (120 µL per well) and allowed to solidify at room temperature for 10-20 min. Samples were subsequently incubated at 37 °C.

Colony-forming unit counting. To determine the viable cell counts, bacterial suspensions were serially diluted by tenfold in sterile PBS. Ten-microliter aliquots of the appropriate dilutions were spotted on agar plates and allowed to air-dry under sterile conditions. The plates were subsequently covered and inverted (to avoid dripping of condensate water onto the agar surface), and incubated at 37 °C for 16-24 h. Colonies were enumerated from spots that satisfied a statistically reliable range (typically between 5 and 50 colonies), and the total viable cell density was calculated and expressed as CFU per milliliter.

Measurement of extracellular pH. For planktonic cultures, extracellular pH was measured directly with the supernatant using a PB-10 pH meter (Sartorius). For biofilms, extracellular pH was

determined ratiometrically using the pH-sensitive fluorescent dye BCECF (MedChemExpress). A standard curve was generated using M9 plus MOPS buffers adjusted to pH values ranging from 4.0 to 9.0 (0.5-unit increments). Fluorescence intensities were measured at Ex/Em = 490/535 nm and 440/535 nm respectively using a microplate reader (every 30-60 min). The fluorescence ratio (490/440) was plotted against pH and fitted to the following Boltzmann sigmoidal equation[57]:

$$\mathrm{pH} = \mathrm{pH}_0 + \mathrm{dpH}\frac{(R_{\min} - R)}{(R - R_{\max})}$$

where R is the measured fluorescence ratio, and pH is the corresponding pH of the M9-MOPS buffer. The parameters $R_{\min}$ and $R_{\max}$ denote the asymptotic minimum and maximum fluorescence ratios, representing the fully protonated (extremely acidic) and fully deprotonated (extremely alkaline) states of the probe, respectively; pH_0 indicates the midpoint pH of the curve where the ratio equals the average of the minimum and maximum values; and dpH represents the slope factor, which dictates the sensitivity of the probe's response to pH changes near the inflection point.

pH perturbation. To manipulate the extracellular pH, MOPS (Macklin) was utilized to buffer the microenvironment. A 100 mM MOPS stock solution was prepared, and the pH was adjusted to either 10.5 or 5.5 using NaOH. After the biofilms reached stationary phase, 60 µL of the appropriate MOPS buffer was added directly to the culture wells in the 96-well plate. For control, 60 µL of NaCl solution were added to the corresponding wells.

Biofilm dispersion. The agarose block biofilms were dispersed by repeatedly pipetting the agarose in the 96-well plate with sterile NaCl solution (0.85% w/v, to match the osmolarity of the M9 medium) until a homogeneous suspension was achieved (taking ~0.5-1 min per well). Microscopic examinations were performed to confirm that the biofilms were dispersed to individual cells.

Biofilm supernatant extraction. Biofilms in each well were dispersed with NaCl solution from an initial agarose volume of 120 µL to a final suspension of 480 µL. The suspension was centrifuged at 10,000 x *g* for 2 min at 4 °C to remove cells and agarose debris. The resulting supernatant was then filtered through a 0.22 µm nylon membrane. Then the supernatant was used immediately or stored at -20 °C.

Measuring extracellular metabolites. Metabolites in biofilm supernatants were quantified using the Agilent 1260 Infinity HPLC system equipped with the Bio-Rad Aminex HPX-87H Ion Exclusion Column (300 × 7.8 mm, 9 µm) and the Micro-Guard Cation H guard column. The mobile phase was 5 mM H_2SO_4 (filtered and degassed) delivered isocratically at 0.6 mL/min with a column temperature of 50 °C. The injection volume was 10 µL. Detection was performed using a diode array detector (DAD) at 210 nm. Metabolites were identified by retention time comparison with standards and quantified using external calibration curves based on peak areas. Standard solutions of acetate, lactate, formate, pyruvate, and succinate were prepared in deionized water (20 mM stocks).

Antibiotic susceptibility assays for biofilms. Biofilms were cultured for 36 h and then treated with antibiotics. The antibiotics were prepared by diluting stock solutions (≥100×) in sterile NaCl solution (0.85% w/v, to match the osmolarity of the M9 medium). For supernatant supplementation experiments, sterile-filtered biofilm supernatants were used in place of the NaCl solution to prepare the antibiotic solutions. For metabolite supplementation experiments, sodium acetate (Macklin), sodium formate (Macklin), succinate (Sigma), glyoxylate (Sigma), and sodium fumarate (Sigma) were prepared as aqueous stock solutions, adjusted to pH 7.0, and sterile-filtered. Unless otherwise specified, metabolites were supplemented to a final concentration of 20 mM. 60 µL of antibiotics were added to each well of the 96-well plate to achieve designated final concentrations (ampicillin, 50 µg/mL; gentamicin, 128 µg/mL; ciprofloxacin, 0.5 µg/mL). For no-antibiotic control, a 60 µL of NaCl solution were added to each well. After 24 h of antibiotic treatment, the biofilms in each well were dispersed into individual cells with NaCl solution from an initial agarose volume of 120 µL into a final suspension of 480 µL. The suspension was then used for viable cell counting. Survival rates were calculated as the ratio of viable cells at the time of sampling to the initial cell count prior to antibiotic treatment.

Antibiotic susceptibility assay for planktonic bacteria. Bacteria were cultured in 96-well plates with M9 medium at 37 °C under continuous shaking for 36 h. The cultures were then treated with antibiotics (ampicillin, 50 µg/mL; gentamicin, 128 µg/mL; ciprofloxacin, 0.5 µg/mL). For metabolite supplementation experiments, sodium acetate was supplemented to a final concentration of 20 mM. For control, 60 µL of NaCl solution were added to the corresponding wells. At designated time points,

aliquots were taken, centrifuged, washed twice with PBS, and serially diluted. Viable cell counts were determined by spotting the dilutions onto antibiotic-free agar plates and incubating at 37 °C for 16-24 h. The resulting CFU counts were used to calculate the survival rates.

pH-dependence of time-kill kinetics of planktonic bacteria. Bacteria were cultured in M9 medium to the exponential growth phase. The culture was centrifuged at 5,000 × *g*, the supernatant was discarded, and the resulting cell pellet was washed twice by resuspension in PBS. The washed cells were subsequently inoculated into fresh M9 media—pre-adjusted to a predefined pH gradient (6.5 and 7.0) using MOPS buffer (100 mM)—to achieve an initial bacterial density of 1~2 × 10^8 CFU/mL. The cultures were then treated with either gentamicin (8 μg/mL) or ciprofloxacin (0.2 μg/mL) and incubated at 37 °C under continuous shaking. At designated time points (0, 0.25, 0.5, 1, 2, and 4 h), 10 μL aliquots were extracted, serially diluted in PBS, and plated onto antibiotic-free agar for viable cell counting. The resulting CFU counts were used to plot the time-kill kinetics.

Testing of the oxygen sensor. The *E. coli* strain harboring the P_{fnrF8}-DL5 reporter plasmid was cultured in M9 medium at 37 °C until reaching an early exponential phase (OD_{600} ≈ 0.2). The medium was supplemented with chloramphenicol (15 μg/mL) to maintain plasmid stability, along with malachite green (MG, 5 μM) as the fluorogen ligand. The culture was then divided into two equal aliquots. One aliquot was transferred into an anaerobic chamber for continued cultivation under strictly anaerobic conditions, while the other aliquot was maintained under standard aerobic conditions with continuous shaking. After 6 h of incubation, cell samples were harvested for imaging. Single-cell fluorescence imaging was subsequently performed using agarose pads to acquire phase-contrast and fluorescence (Cy5 channel, Ex: 646 nm, Em: 662 nm) images using the 60× objective.

Biofilm imaging and analysis. Biofilms were imaged using the Olympus IX83 microscope with Tokai Hit thermal box, X-Cite XYLIS light source, and Andor Zyla 4.2 sCMOS camera. A 10× objective lens was used. For time-lapse microscopy, images were taken every 20-30 min, and the thermal box temperature was kept at 37 °C. For visualization of anaerobic zones in the biofilms, the DL5 oxygen-sensor strain was used, with the addition of chloramphenicol (15 μg/mL) to maintain the plasmid. The DL5 ligand malachite green (5 μM) were added to the medium prior to agarose solidification.

Once the biofilms became visible under the microscope (~10 µm in diameter), phase-contrast and fluorescence (Cy5 channel, Ex: 646 nm, Em: 662 nm) images were acquired every 20 min using the 10× objective (focal plane set to the center of each biofilm). Image analysis was performed using ImageJ and MATLAB. Raw images were split into separate channels, and drift was corrected using the Image Stabilizer plugin in ImageJ. Using phase-contrast images, biofilms were segmented from the background based on a brightness threshold (2× of the background). The projected area of a biofilm was calculated by multiplying the number of pixels in the segmented biofilm and the area of a single pixel. The volume of a biofilm was calculated using its projected area, taking advantage of the fact that the biofilms are spherical.

Statistical analysis. Data are presented as mean ± standard deviation from at least three independent biological replicates. Statistical significance was determined using two-tailed unpaired Student's *t*-test for comparisons between two groups, or one-way ANOVA followed by Dunnett's multiple-comparisons test for comparisons involving more than two groups.

Acknowledgements

We thank the Tsinghua University Center of Pharmaceutical Technology for assistance on the metabolomics experiments. J.L. was supported by the National Key R&D Program of China (2023YFC2306300), the SXMU-Tsinghua Collaborative Innovation Center for Frontier Medicine, and the Tsinghua University Initiative Scientific Research Program.

Author contributions

S.H. and J.L. designed the research. S.H. performed the experiments. Y.Z. contributed to the construction and testing of the oxygen sensor. S.H. and J.L. analyzed the data. S.H. and J.L. wrote the manuscript.

Competing interests

The authors declare no competing interests.

References

[1] Darby, E. M., Trampari, E., Siasat, P., Gaya, M. S., Alav, I., Webber, M. A. & Blair, J. M. A. Molecular mechanisms of antibiotic resistance revisited. *Nat. Rev. Microbiol.* **21**, 280–295 (2023).

[2] Lewis, K. The science of antibiotic discovery. *Cell* **181**, 29–45 (2020).

[3] Durand-Reville, T. F., Miller, A. A., O'Donnell, J. P., Wu, X., Sylvester, M. A., Guler, S., Iyer, R., Shapiro, A. B., Carter, N. M., Velez-Vega, C., Moussa, S. H., McLeod, S. M., Chen, A., Tanudra, A. M., Zhang, J., Comita-Prevoir, J., Romero, J. A., Huynh, H., Ferguson, A. D., Horanyi, P. S., Mayclin, S. J., Heine, H. S., Drusano, G. L., Cummings, J. E., Slayden, R. A. & Tommasi, R. A. Rational design of a new antibiotic class for drug-resistant infections. *Nature* **597**, 698–702 (2021).

[4] Wong, F., Zheng, E. J., Valeri, J. A., Donghia, N. M., Anahtar, M. N., Omori, S., Li, A., Cubillos-Ruiz, A., Krishnan, A., Jin, W. G., Manson, A. L., Friedrichs, J., Helbig, R., Hajian, B., Fiejtek, D. K., Wagner, F. F., Soutter, H. H., Earl, A. M., Stokes, J. M., Renner, L. D. & Collins, J. J. Discovery of a structural class of antibiotics with explainable deep learning. *Nature* **626**, 177–185 (2024).

[5] Jangra, M., Travin, D. Y., Aleksandrova, E. V., Kaur, M., Darwish, L., Koteva, K., Klepacki, D., Wang, W., Tiffany, M., Sokaribo, A., Chen, X., Deng, Z., Tao, M., Coombes, B. K., Vazquez-Laslop, N., Polikanov, Y. S., Mankin, A. S. & Wright, G. D. A broad-spectrum lasso peptide antibiotic targeting the bacterial ribosome. *Nature* **640**, 1022–1030 (2025).

[6] Lewis, K. Persister cells, dormancy and infectious disease. *Nat. Rev. Microbiol.* **5**, 48–56 (2007).

[7] Baym, M., Lieberman, T. D., Kelsic, E. D., Chait, R., Gross, R., Yelin, I. & Kishony, R. Spatiotemporal microbial evolution on antibiotic landscapes. *Science* **353**, 1147–1151 (2016).

[8] Windels, E. M., Michiels, J. E., Fauvart, M., Wenseleers, T., Van den Bergh, B. & Michiels, J. Bacterial persistence promotes the evolution of antibiotic resistance by increasing survival and mutation rates. *ISME J.* **13**, 1239–1251 (2019).

[9] Sauer, K., Stoodley, P., Goeres, D. M., Hall-Stoodley, L., Burmolle, M., Stewart, P. S. & Bjarnsholt, T. The biofilm life cycle: expanding the conceptual model of biofilm formation. *Nat. Rev. Microbiol.* **20**, 608–620 (2022).

[10] Stewart, P. S. & Costerton, J. W. Antibiotic resistance of bacteria in biofilms. *Lancet* **358**, 135–138 (2001).

[11] Ciofu, O., Moser, C., Jensen, P. O. & Hoiby, N. Tolerance and resistance of microbial biofilms. *Nat. Rev. Microbiol.* **20**, 621–635 (2022).

[12] Cao, B., Christophersen, L., Thomsen, K., Sonderholm, M., Bjarnsholt, T., Jensen, P. O., Hoiby, N. & Moser, C. Antibiotic penetration and bacterial killing in a *Pseudomonas aeruginosa* biofilm model. *J. Antimicrob. Chemother.* **70**, 2057–2063 (2015).

[13] Ciofu, O. & Tolker-Nielsen, T. Tolerance and resistance of *Pseudomonas aeruginosa* biofilms to antimicrobial agents-how *Pseudomonas aeruginosa* can escape antibiotics. *Front. Microbiol.* **10**, 913 (2019).

[14] Christophersen, L., Schwartz, F. A., Lerche, C. J., Svanekjaer, T., Kragh, K. N., Laulund, A. S., Thomsen, K., Henneberg, K. A., Sams, T., Hoiby, N. & Moser, C. *In vivo* demonstration of *Pseudomonas aeruginosa* biofilms as independent pharmacological microcompartments. *J.*

Cyst. Fibros. **19**, 996–1003 (2020).

[15] Tuomanen, E., Cozens, R., Tosch, W., Zak, O. & Tomasz, A. The rate of killing of *Escherichia coli* by beta-lactam antibiotics is strictly proportional to the rate of bacterial growth. *J. Gen. Microbiol.* **132**, 1297–1304 (1986).

[16] Dayton, H., Kiss, J., Wei, M., Chauhan, S., LaMarre, E., Cornell, W. C., Morgan, C. J., Janakiraman, A., Min, W., Tomer, R., Price-Whelan, A., Nirody, J. A. & Dietrich, L. E. P. Cellular arrangement impacts metabolic activity and antibiotic tolerance in *Pseudomonas aeruginosa* biofilms. *PLoS Biol.* **22**, e3002205 (2024).

[17] Dwyer, D. J., Belenky, P. A., Yang, J. H., MacDonald, I. C., Martell, J. D., Takahashi, N., Chan, C. T., Lobritz, M. A., Braff, D., Schwarz, E. G., Ye, J. D., Pati, M., Vercruysse, M., Ralifo, P. S., Allison, K. R., Khalil, A. S., Ting, A. Y., Walker, G. C. & Collins, J. J. Antibiotics induce redox-related physiological alterations as part of their lethality. *Proc. Natl. Acad. Sci. USA* **111**, e2100–2109 (2014).

[18] Kolpen, M., Mousavi, N., Sams, T., Bjarnsholt, T., Ciofu, O., Moser, C., Kuhl, M., Hoiby, N. & Jensen, P. O. Reinforcement of the bactericidal effect of ciprofloxacin on *Pseudomonas aeruginosa* biofilm by hyperbaric oxygen treatment. *Int. J. Antimicrob. Agents* **47**, 163–167 (2016).

[19] Nguyen, D., Joshi-Datar, A., Lepine, F., Bauerle, E., Olakanmi, O., Beer, K., McKay, G., Siehnel, R., Schafhauser, J., Wang, Y., Britigan, B. E. & Singh, P. K. Active starvation responses mediate antibiotic tolerance in biofilms and nutrient-limited bacteria. *Science* **334**, 982–986 (2011).

[20] Stewart, P. S., Franklin, M. J., Williamson, K. S., Folsom, J. P., Boegli, L. & James, G. A. Contribution of stress responses to antibiotic tolerance in *Pseudomonas aeruginosa* biofilms. *Antimicrob. Agents Chemother* **59**, 3838–3847 (2015).

[21] Liu, J., Prindle, A., Humphries, J., Gabalda-Sagarra, M., Asally, M., Lee, D. Y., Ly, S., Garcia-Ojalvo, J. & Suel, G. M. Metabolic co-dependence gives rise to collective oscillations within biofilms. *Nature* **523**, 550–554 (2015).

[22] Meredith, H. R., Srimani, J. K., Lee, A. J., Lopatkin, A. J. & You, L. Collective antibiotic tolerance: mechanisms, dynamics and intervention. *Nat. Chem. Biol.* **11**, 182–188 (2015).

[23] Qin, B., Fei, C., Bridges, A. A., Mashruwala, A. A., Stone, H. A., Wingreen, N. S. & Bassler, B. L. Cell position fates and collective fountain flow in bacterial biofilms revealed by light-sheet microscopy. *Science* **369**, 71–77 (2020).

[24] Wang, Z., Zeng, L., Hu, S., Hu, Q., Zhang, Y. & Liu, J. Community-specific cell death sustains bacterial expansion under phosphorus starvation. *Nat. Chem. Biol.* **21**, 867–875 (2025).

[25] Wessel, A. K., Arshad, T. A., Fitzpatrick, M., Connell, J. L., Bonnecaze, R. T., Shear, J. B. & Whiteley, M. Oxygen limitation within a bacterial aggregate. *mBio* **5**, e00992 (2014).

[26] Zhang, Y., Cai, Y., Jin, X., Wu, Q., Bai, F. & Liu, J. Persistent glucose consumption under antibiotic treatment protects bacterial community. *Nat. Chem. Biol.* **21**, 238–246 (2025).

[27] Jo, J., Price-Whelan, A. & Dietrich, L. E. P. Gradients and consequences of heterogeneity in biofilms. *Nat. Rev. Microbiol.* **20**, 593–607 (2022).

[28] Wang, T., Shen, P., He, Y., Zhang, Y. & Liu, J. Spatial transcriptome uncovers rich coordination of metabolism in *Escherichia coli* K12 biofilm. *Nat. Chem. Biol.* **19**, 940–950 (2023).

[29] Zhang, Q., Li, J., Nijjer, J., Lu, H., Kothari, M., Alert, R., Cohen, T. & Yan, J. Morphogenesis and

cell ordering in confined bacterial biofilms. *Proc. Natl. Acad. Sci. USA* **118**, e2107107118 (2021).

[30] Liang, Z., Nilsson, M., Kragh, K. N., Hedal, I., Alcacer-Almansa, J., Kiilerich, R. O., Andersen, J. B. & Tolker-Nielsen, T. The role of individual exopolysaccharides in antibiotic tolerance of *Pseudomonas aeruginosa* aggregates. *Front. Microbiol.* **14**, 1187708 (2023).

[31] Horak, R. D., Ciemniecki, J. A. & Newman, D. K. Bioenergetic suppression by redox-active metabolites promotes antibiotic tolerance in *Pseudomonas aeruginosa*. *Proc. Natl. Acad. Sci. USA* **121**, e2406555121 (2024).

[32] Jo, J., Price-Whelan, A. & Dietrich, L. E. P. Gradients and consequences of heterogeneity in biofilms. *Nat. Rev. Microbiol.* **20**, 593–607 (2022).

[33] Stewart, P. S. & Franklin, M. J. Physiological heterogeneity in biofilms. *Nat. Rev. Microbiol.* **6**, 199–210 (2008).

[34] Clark, D. P. The fermentation pathways of *Escherichia coli*. *FEMS Microbiol. Rev.* **5**, 223–234 (1989).

[35] Tran, P., Lander, S. M. & Prindle, A. Active pH regulation facilitates *Bacillus subtilis* biofilm development in a minimally buffered environment. *mBio* **15**, e0338723 (2024).

[36] Knappe, J. & Sawers, G. A radical-chemical route to acetyl-CoA: the anaerobically induced pyruvate formate-lyase system of *Escherichia coli*. *FEMS Microbiol. Rev.* **6**, 383–398 (1990).

[37] Wolfe, A. J. The acetate switch. *Microbiol. Mol. Biol. Rev.* **69**, 12–50 (2005).

[38] Ishak, A., Mazonakis, N., Spernovasilis, N., Akinosoglou, K. & Tsioutis, C. Bactericidal versus bacteriostatic antibacterials: clinical significance, differences and synergistic potential in clinical practice. *J. Antimicrob. Chemother.* **80**, 1–17 (2025).

[39] Mayers, J. R., Varon, J., Zhou, R. R., Daniel-Ivad, M., Beaulieu, C., Bhosle, A., Glasser, N. R., Lichtenauer, F. M., Ng, J., Vera, M. P., Huttenhower, C., Perrella, M. A., Clish, C. B., Zhao, S. D., Baron, R. M. & Balskus, E. P. A metabolomics pipeline highlights microbial metabolism in bloodstream infections. *Cell* **187**, 4095–4112 (2024).

[40] Patel, R., Singh, G., Kajal, K., Nandini, Alam, P., Kharkwal, H. & Chander, S. Exploring FabH inhibitors for antimicrobial therapy: medicinal chemistry, synthetic approaches, and SAR evaluation. *Mol. Divers.* (2025).

[41] Oh, M. K., Rohlin, L., Kao, K. C. & Liao, J. C. Global expression profiling of acetate-grown *Escherichia coli*. *J. Biol. Chem.* **277**, 13175–13183 (2002).

[42] Shimada, T., Nakazawa, K., Tachikawa, T., Saito, N., Niwa, T., Taguchi, H. & Tanaka, K. Acetate overflow metabolism regulates a major metabolic shift after glucose depletion in *Escherichia coli*. *FEBS Lett.* **595**, 2047–2056 (2021).

[43] Maloy, S. R., Bohlander, M. & Nunn, W. D. Elevated levels of glyoxylate shunt enzymes in *Escherichia coli* strains constitutive for fatty acid degradation. *J. Bacteriol.* **143**, 720–725 (1980).

[44] Peng, B., Su, Y. B., Li, H., Han, Y., Guo, C., Tian, Y. M. & Peng, X. X. Exogenous alanine and/or glucose plus kanamycin kills antibiotic-resistant bacteria. *Cell Metab.* **21**, 249–262 (2015).

[45] Meylan, S., Porter, C. B. M., Yang, J. H., Belenky, P., Gutierrez, A., Lobritz, M. A., Park, J., Kim, S. H., Moskowitz, S. M. & Collins, J. J. Carbon sources tune antibiotic susceptibility in *Pseudomonas aeruginosa* via tricarboxylic acid cycle control. *Cell. Chem. Biol.* **24**, 195–206 (2017).

[46] Bekker, M., de Vries, S., Ter Beek, A., Hellingwerf, K. J. & de Mattos, M. J. Respiration of *Escherichia coli* can be fully uncoupled via the nonelectrogenic terminal cytochrome bd-II oxidase. *J. Bacteriol.* **191**, 5510–5517 (2009).

[47] Prentice, J. A., Kasivisweswaran, S., van de Weerd, R. & Bridges, A. A. Biofilm dispersal patterns revealed using far-red fluorogenic probes. *PLoS Biol.* **22**, e3002928 (2024).

[48] Yang, S., Guo, C. H., Tong, W. Y., Liu, X. Y., Li, J. C. & Kang, M. Identification and characterization of anaerobically activated promoters in *Escherichia coli*. *J. Biotechnol.* **402**, 30–38 (2025).

[49] Taber, H. W., Mueller, J. P., Miller, P. F. & Arrow, A. S. Bacterial uptake of aminoglycoside antibiotics. *Microbiol. Rev.* **51**, 439–457 (1987).

[50] Unden, G. & Bongaerts, J. Alternative respiratory pathways of *Escherichia coli*: energetics and transcriptional regulation in response to electron acceptors. *Biochim. Biophys. Acta* **1320**, 217–234 (1997).

[51] Cecchini, G., Schroder, I., Gunsalus, R. P. & Maklashina, E. Succinate dehydrogenase and fumarate reductase from *Escherichia coli*. *Biochim. Biophys. Acta* **1553**, 140–157 (2002).

[52] Allison, K. R., Brynildsen, M. P. & Collins, J. J. Metabolite-enabled eradication of bacterial persisters by aminoglycosides. *Nature* **473**, 216–220 (2011).

[53] Stokes, J. M., Lopatkin, A. J., Lobritz, M. A. & Collins, J. J. Bacterial metabolism and antibiotic efficacy. *Cell Metab.* **30**, 251–259 (2019).

[54] Ahmad, M., Aduru, S. V., Smith, R. P., Zhao, Z. & Lopatkin, A. J. The role of bacterial metabolism in antimicrobial resistance. *Nat. Rev. Microbiol.* **23**, 439–454 (2025).

[55] Baba, T., Ara, T., Hasegawa, M., Takai, Y., Okumura, Y., Baba, M., Datsenko, K. A., Tomita, M., Wanner, B. L. & Mori, H. Construction of *Escherichia coli* K-12 in-frame, single-gene knockout mutants: the Keio collection. *Mol. Syst. Biol.* **2**, 2006 0008 (2006).

[56] Yamamoto, N., Nakahigashi, K., Nakamichi, T., Yoshino, M., Takai, Y., Touda, Y., Furubayashi, A., Kinjyo, S., Dose, H., Hasegawa, M., Datsenko, K. A., Nakayashiki, T., Tomita, M., Wanner, B. L. & Mori, H. Update on the Keio collection of *Escherichia coli* single-gene deletion mutants. *Mol. Syst. Biol.* **5**, 335 (2009).

[57] Gjetting, K. S., Ytting, C. K., Schulz, A. & Fuglsang, A. T. Live imaging of intra- and extracellular pH in plants using pHusion, a novel genetically encoded biosensor. *J. Exp. Bot.* **63**, 3207–3218 (2012).

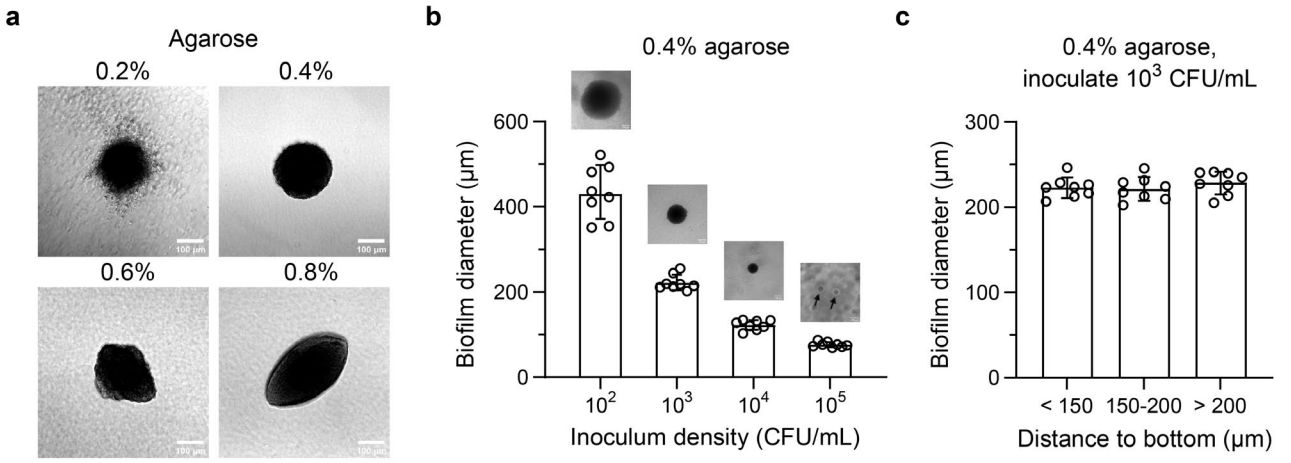

626 **Extended Data Fig. 1: Optimization of the agarose block biofilm assay. a**, Dependence of biofilm
627 morphology on agarose concentration. *E. coli* forms spherical biofilms with well-defined boundaries
628 at an optimal 0.4% (w/v) agarose concentration. Scale bar, 100 μm. **b**, Relationship between initial
629 seeding density and final biofilm size. High inoculation density restricts individual biofilm size. **c**,
630 Uniformity of biofilm growth across system depth. Biofilm sizes remain consistent regardless of their
631 vertical distance from the well bottom in a 120 μL (~375 μm) culture volume. *n* = 8 biological replicates
632 (**b**, **c**). Error bars indicate mean values +/- SD.
633

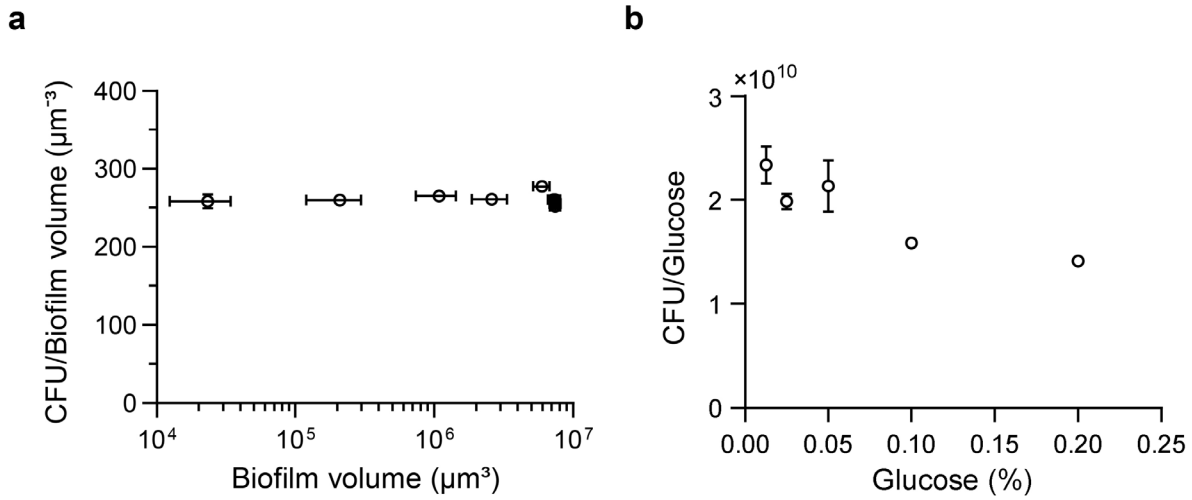

634 **Extended Data Fig. 2: Relation between CFU and biofilm volume or initial glucose. a**, Relationship
635 between CFU and biofilm volume. The ratio of CFU to biofilm volume remains constant across
636 different final biofilm sizes. **b**, Ratio of stationary-phase CFU to initial glucose concentration. The
637 consistent yield efficiency at lower glucose levels (<0.2%, w/v) demonstrates that final biomass is
638 proportional to available carbon. *n* = 3 biological replicates for all the experiments. Error bars indicate
639 mean values +/- SD.
640

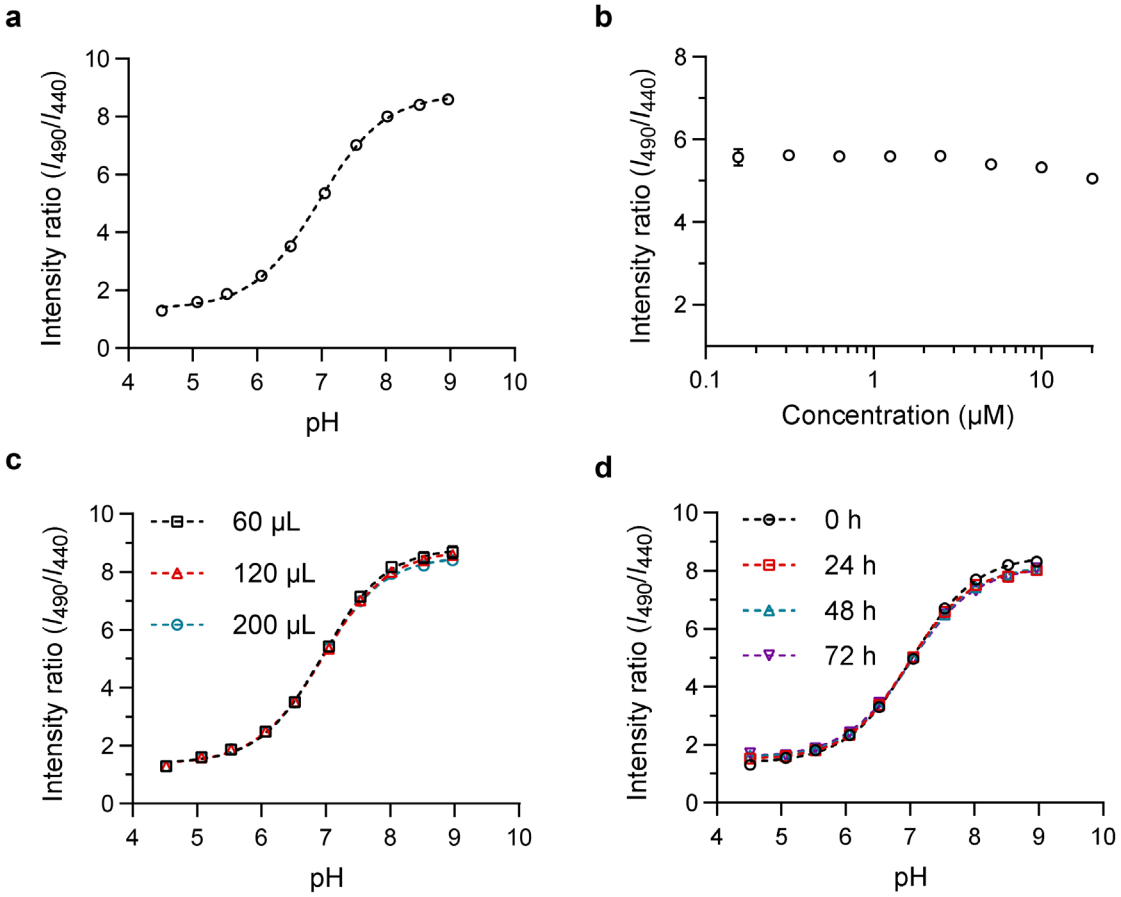

Extended Data Fig. 3: Calibration of the ratiometric pH probe BCECF. a, Calibration standard curve of the BCECF sensor. The plot displays the fluorescence emission ratio at 535 nm (following excitation at 490 nm versus 440 nm) across reference buffers with predefined pH values. The data are strictly fitted to a Boltzmann sigmoidal equation (R^2 = 0.9989). **b**–**d**, Stability of the BCECF ratiometric readout. The excitation ratio is unaffected by variations in total dye concentration (**b**). The pH calibration profiles remain identical across varying culture volumes (60, 120, and 200 µL) (**c**) and after continuous incubation at 37 °C for up to 72 h (**d**). *n* = 3 biological replicates for all the experiments. Error bars indicate mean values +/- SD.

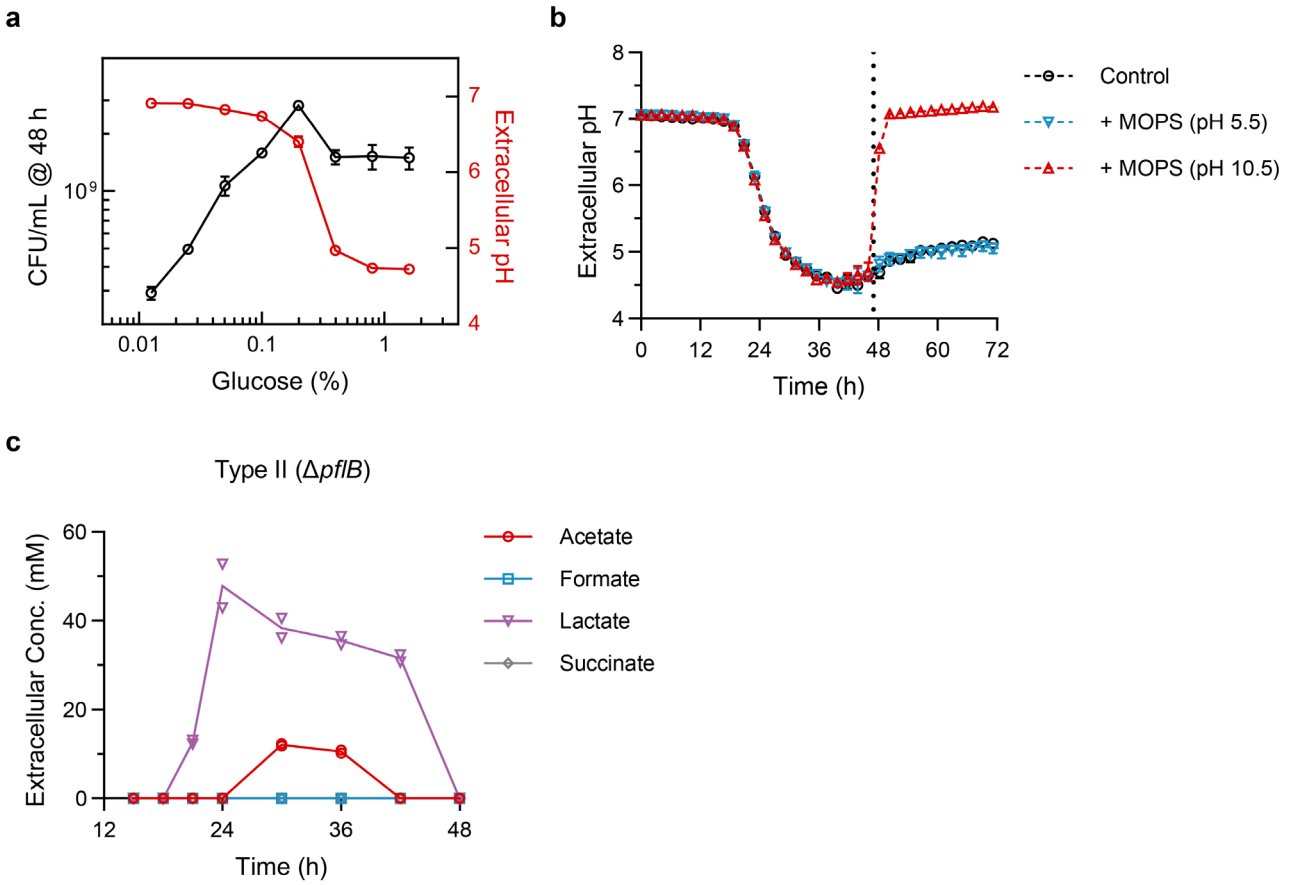

Extended Data Fig. 4: Profiling and perturbation of extracellular environment. **a**, Relationship between glucose-dependent biomass restriction and extracellular pH. The non-monotonic decline in biofilm CFU (left y-axis, 48 h) coincides with environmental acidification (right y-axis). **b**, Effect of MOPS buffer on the type II biofilm microenvironment. Adding MOPS buffer (pH 10.5) at stationary phase (48 h) successfully restores extracellular pH to ~7, whereas untreated controls and biofilms treated with acidic MOPS (pH 5.5) maintain an acidic state. **c**, Extracellular metabolite profiling of the Δ*pflB* mutant under type II conditions. Knocking out *pflB* leads to transient accumulation and consumption of lactate (~40 mM) and a minor transient flux of acetate (~10 mM), allowing the pH and biomass to recover. *n* = 3 (**a**, **b**) or 2 (**c**) biological replicates. Error bars indicate mean values +/- SD.

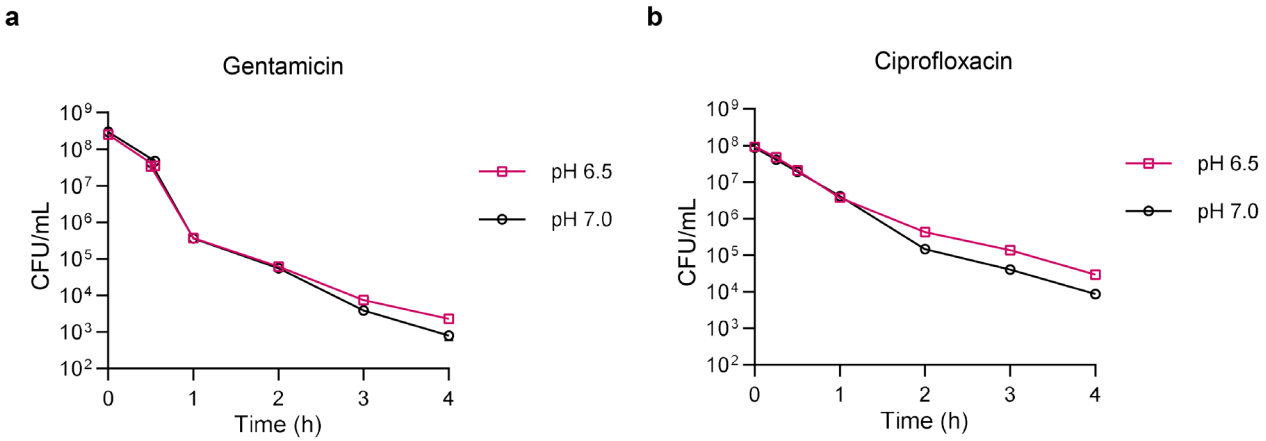

Extended Data Fig. 5: pH dependence of antibiotic efficacy. a, b, Time-kill kinetics of planktonic *E. coli* exposed to gentamicin (8 µg/mL) (**a**) and ciprofloxacin (0.2 µg/mL) (**b**). The bactericidal efficacy of both antibiotics are insensitive to pH change from 7.0 to 6.5. *n* = 3 biological replicates (**a**, **b**). Error bars indicate mean values +/- SD.

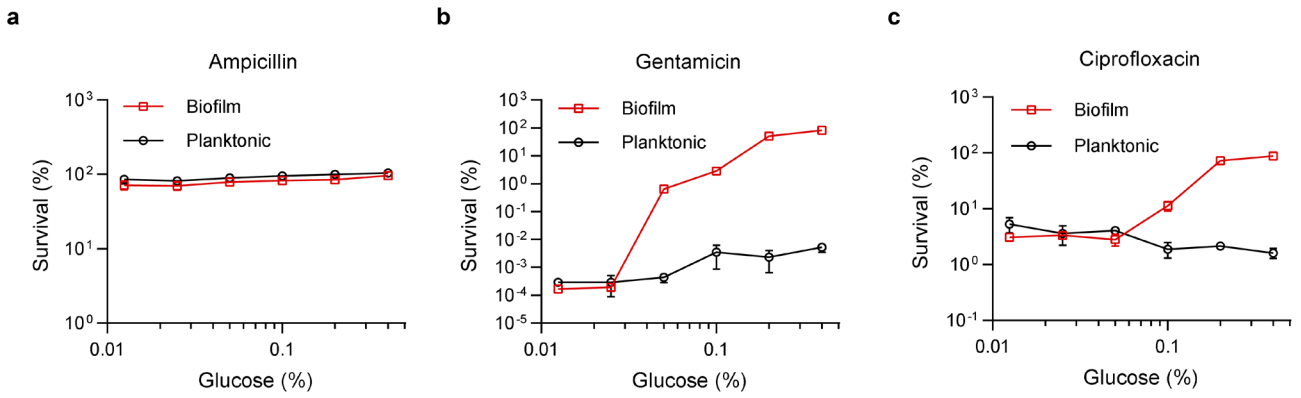

Extended Data Fig. 6: Dependence of antibiotic tolerance on initial glucose. a–c, Survival of bacteria after 24 h of antibiotic treatment (ampicillin, 50 µg/mL; gentamicin, 128 µg/mL; ciprofloxacin, 0.5 µg/mL). Type II biofilms showed high tolerance to gentamicin and ciprofloxacin. Plotted on a logarithmic scale. The planktonic control was performed with the same antibiotic challenge assay. *n* = 3 biological replicates for all the experiments. Error bars indicate mean values +/- SD.

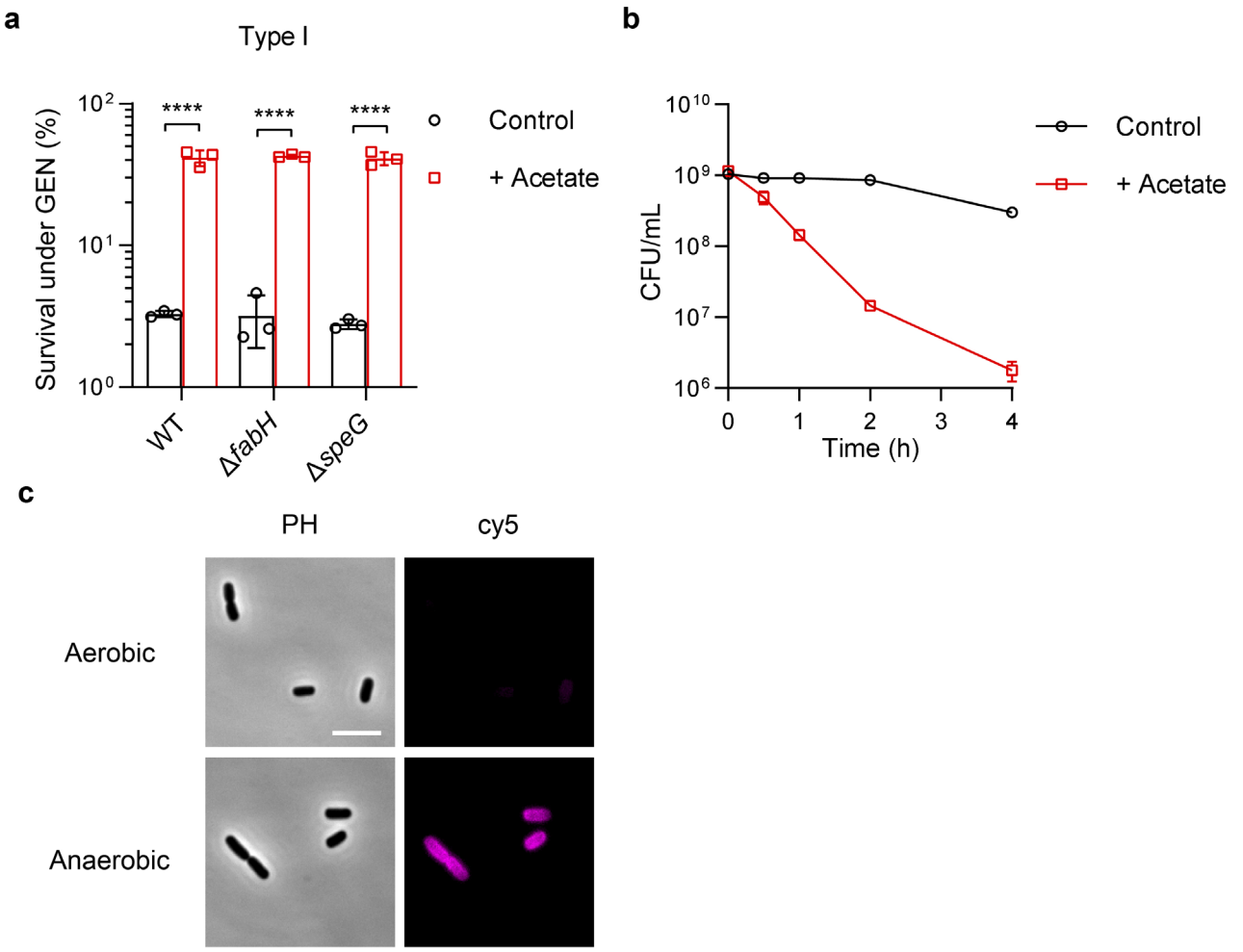

672 **Extended Data Fig. 7: Profiling of bacterial tolerance and the oxygen sensor. a**, Effect of accessory
673 acetyl-CoA assimilation pathways on acetate-induced tolerance. Knocking out fatty acid biosynthesis
674 (Δ*fabH*) or polyamine acetylation (Δ*speG*) pathways does not abolish the protective effect of acetate
675 against gentamicin (128 µg/mL) in type I biofilms. **b**, Effect of acetate on planktonic bacteria.
676 Supplementing acetate enhances gentamicin (128 µg/mL) killing in planktonic cultures, contrasting
677 with its protective role in biofilms. **c**, Validation of the hypoxia sensor. Single-cell fluorescence imaging
678 confirms that the sensor is activated under anaerobic conditions. Scale bar, 5 µm. *n* = 3 biological
679 replicates (**a**, **b**). Error bars indicate mean values +/- SD. Statistical significance was determined by
680 two-tailed unpaired Student's *t*-test (**** $p < 0.0001$).
681

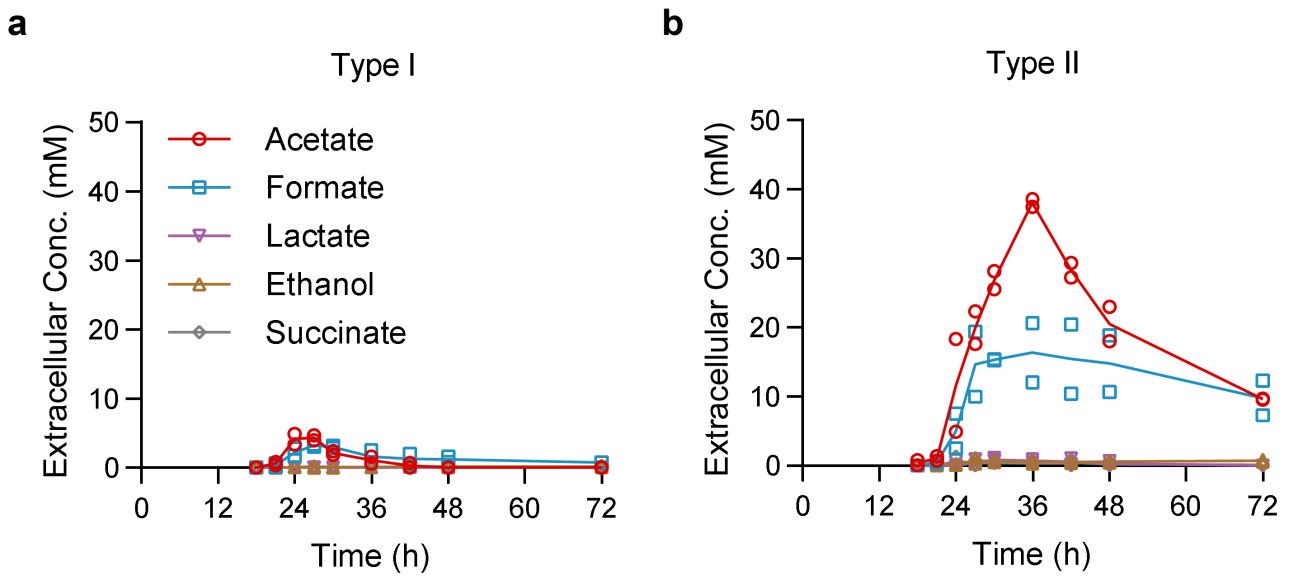

682 **Extended Data Fig. 8: Concentration of extracellular metabolites during the growth of the biofilm**
683 **(with MOPS buffer). a**, **b**, Extracellular metabolite profiling of type I (**a**) and type II (**b**) biofilms
684 cultured with continuous MOPS buffering. Type II biofilms exhibit a biphasic metabolic trajectory
685 where acetate is accumulated and subsequently consumed. *n* = 2 biological replicates (**a**, **b**).
686

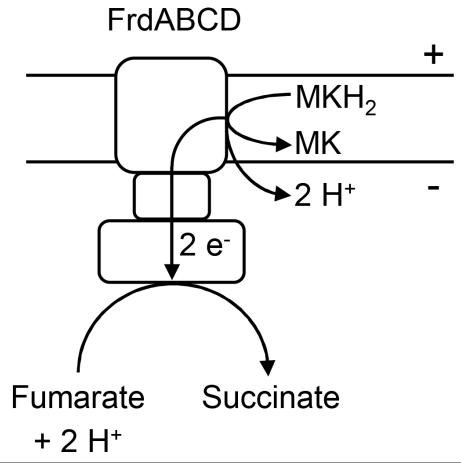

687 **Extended Data Fig. 9: Fumarate acts as electron acceptor.** The fumarate reductase complex (FrdABCD)
688 reduces fumarate to succinate, operating as an alternative electron sink. MK/MKH2:
689 menaquinone/menaquinol.
690

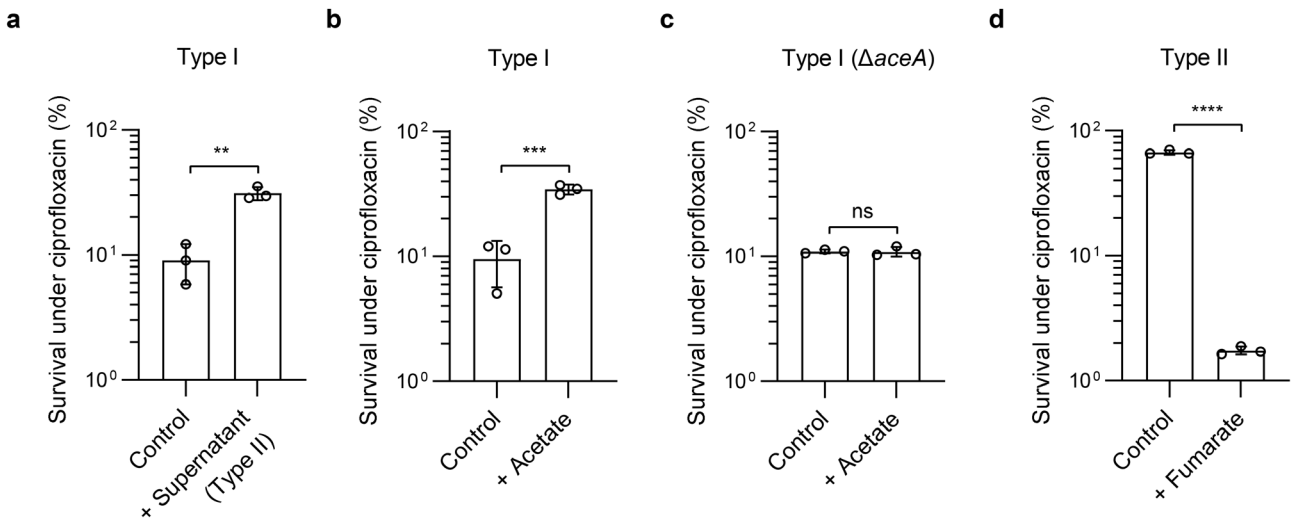

Extended Data Fig. 10: Biofilm tolerance to ciprofloxacin. a–**b**, Effect of type II biofilm supernatant (**a**) or exogenous acetate (**b**) on type I biofilm survival against ciprofloxacin. Both significantly boost the tolerance of type I biofilms. **c**, Effect of the glyoxylate shunt on acetate-induced tolerance. The tolerance-promoting effect of acetate is abolished in the Δ*aceA* mutant. **d**, Effect of fumarate supplementation on ciprofloxacin tolerance in type II biofilms. Providing fumarate as an alternative electron acceptor neutralizes the tolerance. In panels **b**–**d**, ciprofloxacin was applied at a final concentration of 0.5 μg/mL, and exogenous metabolites (acetate and fumarate) were supplemented at 20 mM. *n* = 3 biological replicates for all the experiments. Error bars indicate mean values +/- SD. Statistical significance was determined by two-tailed unpaired Student's *t*-test ($p < 0.01$, *** $p < 0.001$, **** $p < 0.0001$, ns: no significant).